Research Article | Vol. 26, No. 4 | 19 Feb 2018 | OPTICS EXPRESS 3839
Optics EXPRESS

Unidirectional reflectionless phenomena in a non-Hermitian quantum system of quantum dots coupled to a plasmonic waveguide

NAN WU,[1] CONG ZHANG,[1] XING RI JIN,[1,3] YING QIAO ZHANG,[1,4] AND YOUNGPAK LEE[2]

[1]*Department of Physics, College of Science, Yanbian University, Yanji, Jilin 133002, China*
[2]*Quantum Photonic Science Research Center and Department of Physics, Hanyang University, Seoul 133-791, South Korea*
[3]*xrjin@ybu.edu.cn*
[4]*yqzhang@ybu.edu.cn*

Abstract: Unidirectional reflectionless phenomena are investigated theoretically in a non-Hermitian quantum system composed of several quantum dots and a plasmonic waveguide. By adjusting the phase shifts between quantum dots, single- and dual-band unidirectional reflectionlessnesses are realized at exceptional points based on two and three quantum dots coupled to a plasmonic waveguide, respectively. In addition, single- and dual-band unidirectional perfect absorptions with high quality factors are obtained at the vicinity of exceptional points.

OCIS codes: (240.6680) Surface plasmons; (250.5590) Quantum-well, -wire and -dot devices; (270.0270) Quantum optics; (270.1670) Coherent optical effects; (270.5580) Quantum electrodynamics.

References and links

1. C. M. Bender, and S. Boettcher, "Real spectra in non-Hermitian Hamiltonians having PT symmetry," Phys. Rev. Lett. **80**, 5243–5246 (1998).
2. C. M. Bender, "Making sense of non-Hermitian Hamiltonians," Rep. Prog. Phys. **70**, 947–1018 (2007).
3. Y. Choi, S. Kang, S. Lim, W. Kim, J. R. Kim, J. H. Lee, and K. An, "Quasieigenstate coalescence in an atom-cavity quantum composite," Phys. Rev. Lett. **104**, 153601 (2010).
4. J. Xu, Y. X. Du, W. Huang, and D. W. Zhang, "Detecting topological exceptional points in a parity-time symmetric system with cold atoms," Opt. Express **25**, 15786–15795 (2017).
5. J. Wiersig, "Enhancing the sensitivity of frequency and energy splitting detection by using exceptional points: application to microcavity sensors for single-particle detection," Phys. Rev. Lett. **112**, 203901 (2014).
6. Y. Shin, H. Kwak, S. Moon, S. B. Lee, J. Yang, and K. An, "Observation of an exceptional point in a two-dimensional ultrasonic cavity of concentric circular shells," Sci. Rep. **6**, 38826 (2016).
7. A. Regensburger, C. Bersch, M. A. Miri, G. Onishchukov, D. N. Christodoulides, and U. Peschel, "Parity-time synthetic photonic lattices," Nature **488**, 167–171 (2012).
8. S. Longhi, "PT-symmetric laser absorber," Phys. Rev. A **82**, 031801 (2010).
9. Y. Sun, W. Tan, H. Q. Li, J. Li, and H. Chen, "Experimental demonstration of a coherent perfect absorber with PT phase transition," Phys. Rev. Lett. **112**, 143903 (2014).
10. A. Guo, G. J. Salamo, D. Duchesne, R. Morandotti, M. V. Ravat, V. Aimez, G. A. Siviloglou, and D. N. Christodoulides, "Observation of PT-symmetry breaking in complex optical potentials," Phys. Rev. Lett. **103**, 093902 (2009).
11. B. Peng, S. K. Ozdemir, F. Lei, F. Monifi, M. Gianfreda, G. L. Long, S. Fan, F. Nori, C. M. Bender, and L. Yang, "Parity-time-symmetric whispering-gallery microcavities," Nat. Phys. **10**, 394-398 (2014).
12. Z. Lin, H. Ramezani, T. Eichelkraut, T. Kottos, H. Cao, and D. N. Christodoulides, "Unidirectional invisibility induced by PT-symmetric periodic structures," Phys. Rev. Lett. **106**, 213901 (2011).
13. L. Feng, Y. L. Xu, W. S. Fegadolli, M. H. Lu, J. E. B. Oliveira, V. R. Almeida, Y. F. Chen, and A. Scherer, "Experimental demonstration of a unidirectional reflectionless parity-time metamaterial at optical frequencies," Nat. Mater. **12**, 108 (2013).
14. X. T. Gu, R. Bai, C. Zhang, X. R. Jin, Y. Q. Zhang, S. Zhang, and Y. P. Lee, "Unidirectional reflectionless propagation in a non-ideal parity-time metasurface based on far field coupling," Opt. Express **25**, 11778–11787 (2017).
15. R. Bai, C. Zhang, X. Gu, X. R. Jin, Y. Q. Zhang, and Y. P. Lee, "Switching the unidirectional refectionlessness by polarizationin non-ideal PT metamaterial based on the phase coupling," Sci. Rep. **7**, 10742 (2017).
16. C. Zhang, R. Bai, X. Gu, X. R. Jin, Y. Q. Zhang, and Y. P. Lee, "Dual-band unidirectional reflectionless phenomena in an ultracompact non-Hermitian plasmonic waveguide system based on near-field coupling," Opt. Express **25**, 24281–24289 (2017).

#317930 https://doi.org/10.1364/OE.26.003839
Journal © 2018 Received 18 Dec 2017; revised 24 Jan 2018; accepted 25 Jan 2018; published 5 Feb 2018

Optics EXPRESS

17. J. T. Shen, and S. Fan, "Coherent photon transport from spontaneous emission in one-dimensional waveguides," Opt. Lett. **30**, 2001–2003 (2005).
18. W. Chen, G. Y. Chen, and Y. N. Chen, "Coherent transport of nanowire surface plasmons coupled to quantum dots," Opt. Express **18**, 10360–10368 (2010).
19. W. Chen, G. Y. Chen, and Y. N. Chen, "Controlling Fano resonance of nanowire surface plasmons," Opt. Lett. **36**, 3602-3604 (2011).
20. G. Y. Chen, and Y. N. Chen, "Correspondence between entanglement and Fano resonance of surface plasmons," Opt. Lett. **37**, 4023–4025 (2012).
21. X. F. Zang, T. Zhou, B. Cai, and Y. M. Zhu, "Controlling single-photon transport properties in a waveguide coupled with two separated atoms," J. Phys. B: At. Mol. Opt. Phys. **46**, 145504 (2013).
22. D. E. Chang, A. S. Sorensen, E. A. Demler, and M. D. Lukin, "A single-photon transistor using nanoscale surface plasmons," Nat. Phys. **3**, 807–812 (2007).
23. J. T. Shen, and S. Fan, "Theory of single-photon transport in a single-mode waveguide. I. Coupling to a cavity containing a two-level atom," Phys. Rev. A **79**, 023837 (2009).
24. J. T. Shen, and S. Fan, "Theory of single-photon transport in a single-mode waveguide. II. Coupling to a whispering-gallery resonator containing a two-level atom," Phys. Rev. A **79**, 023838 (2009).
25. M. T. Cheng, and Y. Y. Song, "Fano resonance analysis in a pair of semiconductor quantum dots coupling to a metal nanowire," Opt. Lett. **37**, 978-980 (2012).
26. G. Y. Chen, N. Lambert, C. H. Chou, Y. N. Chen, and F. Nori, "Surface plasmons in a metal nanowire coupled to colloidal quantum dots: scattering properties and quantum entanglement," Phys. Rev. B **84**, 045310 (2011).
27. G. Y. Chen, C. M. Li, and Y. N. Chen, "Generating maximum entanglement under asymmetric couplings to surface plasmons," Opt. Lett. **37**, 1337–1339 (2012).
28. N. C. Kim, J. B. Li, Z. J. Yang, Z. H. Hao, and Q. Q. Wang, "Switching of a single prepagating plasmon by two quantum dots system," Appl. Phys. Lett. **97**, 061110 (2010).
29. N. C. Kim, and M. C. Ko, "Switching of a single photon by two Λ-type three-level quantum dots embedded in cavities coupling to one-dimensional waveguide," Plasmonics **10**, 605–610 (2015).
30. N. C. Kim, M. C. Ko, S. I. Choe, C. J. Jang, G. J. Kim, Z. H. Hao, J. B. Li, and Q. Q. Wang, "Interparticle coupling effects of two quantum dots system on the transport properties of a single plasmon," arXiv:1708.06635.
31. N. C. Kim, M. C. Ko, and C. I. Choe, "Scattering of a single plasmon by two-level and V-type three-level quantum dot systems coupled to 1D waveguide," Plasmonics **10**, 1447–1452 (2015).
32. N. C. Kim, M. C. Ko, and Q. Q. Wang, "Single plasmon switching with n quantum dots system coupled to one-dimentional waveguide," Plasmonics **10**, 611–615 (2014).
33. N. C. Kim, M. C. Ko, S. I. Choe, Z. H. Hao, L. Zhou, J. B. Li, S. J. Im, Y. H. Ko, C. G. Jo, and Q. Q. Wang, "Transport properties of a single plasmon interacting with a hybrid exciton of a metal nanoparticle-semiconductor quantum dot system coupled to a plasmonic waveguide," Nanotechnology **27**, 465703 (2016).
34. M. C. Ko, N. C. Kim, S. I. Choe, Z. H. Hao, L. Zhou, J. B. Li, I. G. Kim, and Q. Q. Wang, "Coherent controllable transport of a surface plasmon coupled to a plasmonic waveguide with a metal nanoparticle-semiconductor quantum dot hybrid system," Plasmonics **11**, 1613–1619 (2016).
35. P. C. Kuo, G. Y. Chen, and Y. N. Chen, "Scattering of nanowire surface plasmons coupled to quantum dots with azimuthal angle difference," Sci. Rep. **6**, 37766 (2016).
36. J. J. Chen, C. Wang, R. Zhang, and J. H. Xiao, "Multiple plasmon-induced transparencies in coupled-resonator systems," Opt. Lett. **37**, 5133-5135 (2012).
37. X. R. Jin, Y. Q. Zhang, S. Zhang, Y. P. Lee, and J. Y. Rhee, "Polarization-independent electromagnetically induced transparency-like effects in stacked metamaterials based on Fabry-Pérot resonance," J. Opt. **15**, 125104 (2013).
38. T. Lund-Hansen, S. Stobbe, B. Julsgaard, H. Thyrrestrup, T. Sunner, M. Kamp, A. Forchel, and P. Lodahl, "Experimental realization of highly efficient broadband coupling of single quantum dots to a photonic crystal waveguide," Phys. Rev. Lett. **101**, 113903 (2008).
39. J. Claudon, J. Bleuse, N. S. Malik, M. Bazin, P. Jaffrennou, N. Gregersen, C. Sauvan, P. Lalanne, and G. M. Gérard, "A highly efficient single-photon source based on a quantum dot in a photonic nanowire," Nat. Photon. **4**, 174-177 (2010).
40. Q. Li, H. Wei and H. X. Xu, "Resolving single plasmons generated by multiquantum-emitters on a silver nanowire," Nano. Lett. **14**, 3358–3363 (2014).

1. Introduction

In 1998, Bender and colleagues discovered that the parity-time symmetry non-Hermitian Hamiltonian can describe the real eigenvalues spectra [1, 2]. For non-Hermitian system, an important contribution is the introduction of exceptional point (EP) that is a special point in parameter space of non-Hermitian system where eigenvalues coalesce into only one value. Based on the recent investigations on EP in a wide range of quantum systems [3–6] and classical optical systems [7–16], many interesting phenomena are discovered at EP in classical optical

Optics EXPRESS

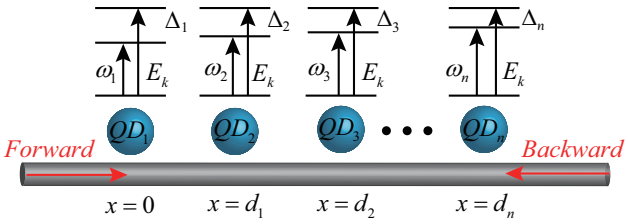

Fig. 1. Schematic of n QDs coupled to a plasmonic waveguide.

systems, such as optical isolation [7], laser [8], coherent perfect absorption [9], non-reciprocal light propagation [10, 11], and unidirectional reflctionlessness [12–16]. In quantum systems, recently, the transport properties of single plasmon or photon in one dimensional waveguide have been investigated in Hermitian [17–21] and non-Hermitian systems [22–35]. In 2007, Chang *et al.* [22] studied the surface plasmon transport properties in non-Hermitian system of nanowire interacting with two-level emitter. Then Shen *et al.* [23, 24] reported the single photon transport properties in non-Hermitian coupling system of two-level emitter and a optical waveguide. Subsequently, Cheng *et al.* [25] analyzed the Fano-type transmission spectrum in a pair of semiconductor quantum dots (QDs) coupling to a metal nanowire. And Chen *et al.* [26, 27] researched the transmission and reflection of surface plasmon and quantum entanglement of two QDs in non-Hermitian system of a metal nanowire coupled to two QDs. Lately, Kim *et al.* investigated the surface plasmon transport properties in non-Hermitian systems consist of two QDs [28–30], three QDs [31], n QDs [32] and metal nanoparticle-QD [33] coupled to a plamonic waveguide, respectively. To date, most of the recent researches focus on the transport properties of single plasmon for one direction in non-Hermitian system of optical waveguide or metal naonwire interacting with QDs. Unidirectional transport properties of surface plasmon in non-Hermitian QDs-plasmonic waveguide coupling system have rarely been reported.

In this work, we investigated the single- and dual-band unidirectional reflectionless phenomena at EPs in non-Hermitian systems composed of two and three unidentical QDs coupled to a plasmonic waveguide, respectively, by appropriately adjusting the phase shifts between QDs. Moreover, we obtained the unidirectional perfect absorptions (UPAs) with high quality factors of ~300 near EPs.

2. Model and calculation

The system of a surface plasmon interacting with n QDs coupled to a plasmonic waveguide is shown in Fig. 1. Under the rotating wave approximation, the non-Hermitian Hamiltonian of the system is given by ($\hbar = 1$)

$$H = \int dx \Big\{ -iv_g C_R^\dagger(x)\frac{\partial}{\partial x}C_R(x) + iv_g C_L^\dagger(x)\frac{\partial}{\partial x}C_L(x) + g\sum_{j=1}^{n}\delta_j(x-d_j)\big[C_R^\dagger(x)\sigma_-^j + C_R(x)\sigma_+^j + C_L^\dagger(x)\sigma_-^j + C_L(x)\sigma_+^j\big]\Big\} + \sum_{j=1}^{n}(\omega_j - i\frac{\Gamma}{2})\sigma_{e_j,e_j}, \tag{1}$$

where $C_R^\dagger(x)$ ($C_L^\dagger(x)$) and $C_R(x)(C_L(x))$ represent a bosonic operator creating and annihilating a right-going (left-going) surface plasmon at x. v_g is the group velocity of the incident surface plasmon. For simplicity, the coupling constants(g) between two QDs and a plasmonic waveguide

Optics EXPRESS

are the same. $\sigma_{e_j,e_j} = |e_j\rangle\langle e_j|$ and $\sigma_+^j = |e_j\rangle\langle g_j|$ represent diagonal element and off-diagonal element of the jth QD operator, respectively. ω_j and $\Gamma/2$ are transition frequency and decay rate of the jth QD. Here, our system is non-Hermitian in view of the decay rate $\Gamma/2$ of QDs.

Assuming that a single surface plasmon is incident from the left or right with energy $E_k = v_g k$ (k is wave vector), the eigenstate of the system can be written as

$$|E_k\rangle = \int dx\Big[\Phi_{k,R}^\dagger(x)C_R^\dagger(x) + \Phi_{k,L}^\dagger(x)C_L^\dagger(x)\Big]|g_1, g_2, ..., g_j\rangle|0\rangle + \sum_{j=1}^{n}\xi_{k_j}\sigma_+^j|g_1, g_2, ..., g_j\rangle|0\rangle, \tag{2}$$

where $|g_1, g_2, ..., g_j\rangle|0\rangle$ describes that j QDs are in the ground states and no surface plasmon is in waveguide. ξ_{k_j} is the probability amplitude that the jth QD absorbs a surface plasmon and jumps to its excited state. For a single surface plasmon incident from left or right, the scattering amplitudes $\Phi_{k,R}^\dagger(x)$ and $\Phi_{k,L}^\dagger(x)$ can be written as ($d_0 = 0$)

$$\begin{aligned}
\Phi_{k,R}^\dagger(x) \equiv& e^{ikx}\Big[\beta(-x) + \sum_{j=2}^{n} a_{j-1}\beta(x - d_{j-2})\beta(d_{j-1} - x) + t\beta(x - d_{j-1})\Big],\\
\Phi_{k,L}^\dagger(x) \equiv& e^{-ikx}\Big[r\beta(-x) + \sum_{j=2}^{n} b_{j-1}\beta(x - d_{j-2})\beta(d_{j-1} - x)\Big],
\end{aligned} \tag{3}$$

where t and r are the transmission and reflection amplitudes, respectively, $e^{ikx}\sum_{j=2}^{n} a_{j-1}\beta(x - d_{j-2})\beta(d_{j-1} - x)$ and $e^{-ikx}\sum_{j=2}^{n} b_{j-1}\beta(x - d_{j-2})\beta(d_{j-1} - x)$ represent the wave function of the surface plasmon between $\sum_{j=2}^{n} d_{j-1}$ and $\sum_{j=2}^{n} d_{j-2}$. $\beta(x)$ is the unit step function. When $x \geq 0$, $\beta(x)$ is equal to unity and zero when $x < 0$.

3. Single-band unidirectional reflectionlessness

Firstly, we consider the case of two QDs coupled to a plasmonic waveguide. The direction of incident surface plasmon from the left (right) is defined as the forward (backward) direction. By solving the eigenvalue equation $H|E_k\rangle = E_k|E_k\rangle$, we obtain the transmission and reflection coefficients for forward and backward directions, as

$$\begin{aligned}
t =& \frac{(\Gamma - 2i\Delta_1)(\Gamma - 2i\Delta_2)}{-16(-1 + e^{2i\theta_1})\eta^2 + 8\eta\big[\Gamma - i(\Delta_1 + \Delta_2)\big] + (\Gamma - 2i\Delta_1)(\Gamma - 2i\Delta_2)},\\
r_f =& -\frac{16(-1 + e^{2i\theta_1})\eta^2 - 4\eta\big[(1 + e^{2i\theta_1})\Gamma - 2i(e^{2i\theta_1}\Delta_1 + \Delta_2)\big]}{16(-1 + e^{2i\theta_1})\eta^2 - 8\eta\big[\Gamma - i(\Delta_1 + \Delta_2)\big] - (\Gamma - 2i\Delta_1)(\Gamma - 2i\Delta_2)},\\
r_b =& -\frac{16(-1 + e^{2i\theta_1})\eta^2 - 4\eta\big[(1 + e^{2i\theta_1})\Gamma - 2i(\Delta_1 + e^{2i\theta_1}\Delta_2)\big]}{16(-1 + e^{2i\theta_1})\eta^2 - 8\eta\big[\Gamma - i(\Delta_1 + \Delta_2)\big] - (\Gamma - 2i\Delta_1)(\Gamma - 2i\Delta_2)},
\end{aligned} \tag{4}$$

where $\eta = g^2/v_g$, $\theta_1 = kd_1$ is the phase shift of surface plasmon between two QDs. $\Delta_{1(2)}$ is the detuning between $QD_{1(2)}$ and incident surface plasmon. Here, we choose the resonance wavelength of $QD_{1(2)}$ in 1540nm(1560nm), it is around the optic fiber communication wavelength(1550nm). t is transmission coefficient, r_f and r_b are reflection coefficients for forward and backward directions, respectively. Here, $T = |t|^2$, $R_f = |r_f|^2$ and $R_b = |r_b|^2$ denote transmission, forward reflection and backward reflection, respectively.

Figure 2 shows the reflection and transmission spectra versus wavelength with the phase shift $\theta_1 = 0.96365\pi$, π and 1.03635π, respectively, when $\Gamma = 0.1\eta$ ($\eta = 1.8 \times 10^{13}$rad/s). From Fig. 2(a) (2(c)), reflections for forward and backward directions at wavelength 1544.69nm (1555.216nm) are ~ 0.8 (~ 0) and ~ 0 (~ 0.8), respectively. That is, the single-band unidirectional

Optics EXPRESS

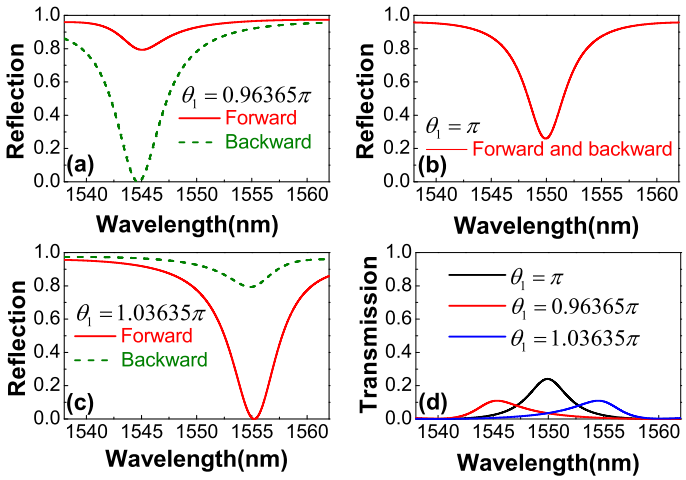

Fig. 2. Reflection spectra for forward and backward directions versus wavelength with phase shifts $\theta_1 = 0.96365\pi$ (a), π (b), and 1.03635π (c), respectively. (d) Transmission spectra versus wavelength with $\theta_1 = \pi$, 0.96365π, and 1.03635π, respectively. Here $\eta = 1.8 \times 10^{13}$rad/s and $\Gamma = 0.1\eta$.

reflectionlessness is obtained, respectively, at 1544.69nm and 1555.216nm (EPs) when phase shift $\theta_1 = 0.96365\pi$ and 1.03635π. While for the phase shift θ_1 is π, reflections for forward and backward directions are the same, shown in Fig. 2(b). Fig. 2(d) shows the transmission spectra with black, red and blue solid lines corresponding to phase shift $\theta_1 = \pi$, 0.96365π and 1.03635π, respectively. We notice that low transmissivity occurs at wavelength 1544.69nm (1555.216nm) for $\theta_1 = 0.96365\pi$ (1.03635π).

In our system, the phase differences between two QDs for forward and backward directions can be expressed as $\phi_f = \phi_1 - \phi_2 + 2\theta_1$ and $\phi_b = \phi_2 - \phi_1 + 2\theta_1$, respectively. Here θ_1 is the phase shift between two QDs. $\phi_{1(2)}$ represents the phase shift for $QD_{1(2)}$, which equals to $(\omega - \omega_{1(2)})/(g^2/v_g + \Gamma/2)$ [17, 36, 37]. By simple calculation, $\phi_f(\phi_b)$ and $\phi_b(\phi_f)$ are $\sim 2\pi$ and $\sim \pi$, respectively, at 1555.216nm and 1544.69nm, resulting in unidirectional reflectionlessness and high reflection based on the Fabry-Pérot resonance as shown in Figs. 2(c) and 2(a).

Next, we further investigate the physics properties of the non-Hermitian quantum system. By using Eq. (4), the scattering matrix S of the non-Hermitian system can be written as

$$S = \begin{pmatrix} t & r_b \\ r_f & t \end{pmatrix}. \tag{5}$$

The eigenvalues of the scattering matrix S can be expressed as

$$s_\pm = t \pm \sqrt{r_f r_b}. \tag{6}$$

When $\sqrt{r_f r_b}$ equals to zero, two eigenvalues coalesce and the EPs occur. In other words, when $r_f = 0$, $r_b \neq 0$ ($r_b = 0$, $r_f \neq 0$), the unidirectional reflectionlessness appears.

Figure 3 shows the real and imaginary parts of the eigenvalues $s_\pm$ of the scattering matrix S as the function of wavelength for $\theta_1 = 0.96365\pi$ ((a), (b)), π ((c), (d)) and 1.03635π ((e),(f)), respectively. From Figs. 3(a) and 3(b) (3(e) and 3(f)), two real parts coalesce at one point while two imaginary parts cross at wavelength 1544.69nm (1555.216nm) when phase shift $\theta_1 = 0.96365\pi$ (1.03635π), which corresponds to the same complex eigenvalues $s_+ = s_-$. In this case, t is complex and $\sqrt{r_f r_b}$ is zero. That is, EPs occur at wavelength 1544.69nm and 1555.216nm when phase shift $\theta_1 = 0.96365\pi$ and 1.03635π, respectively. Therefore, unidirectional reflectionlessness at

Optics EXPRESS

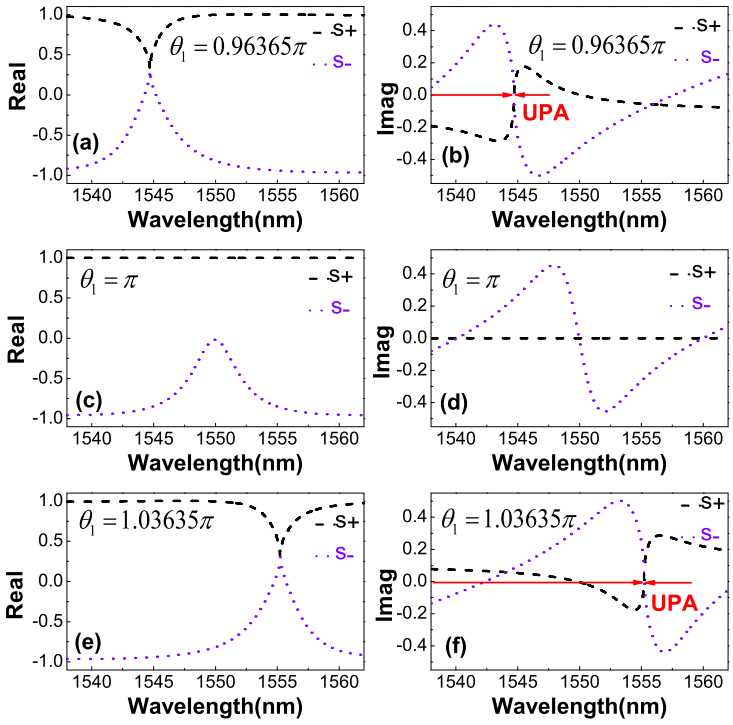

Fig. 3. Real and imaginary parts of the eigenvalues $s_\pm$ as the function of wavelength with different phase shifts $\theta_1 = 0.96365\pi$ (a,b), π (c,d), and 1.03635π (e,f), respectively.

EPs is obtained in the non-Hermitian quantum system by appropriate choosing the phase shift between two QDs. However, when phase shift $\theta_1 = \pi$, two real parts of $s_\pm$ do not coalesce (Fig. 3(c)), while two imaginary parts cross at three points (1540nm, 1549.9nm and 1559.9nm) with the imaginary part of s_+ being zero (Fig. 3(d)). Correspondingly, t is real and $r_f r_b$ is bigger than zero at the three points. In this case, our system is Hermitian. Except for these points, the system is non-Hermitian. That is to say, phase transition from Hermitian to non-Hermitian occurs at 1540nm, 1549.9nm and 1559.9nm when $\theta_1 = \pi$.

When both t and $\sqrt{r_f r_b}$ are complex, we can obtain that one of the eigenvalues $s_\pm$ is real and the other is complex based on some appropriately chosen parameters according to Eq. (6). From Fig. 3(b), one of the imaginary parts of eigenvalues $s_\pm$ is equal to zero at 1544.687nm and 1544.696nm (marked by two red arrows) in the vicinity of EP (1544.69nm), respectively, where the phenomena of UPAs [9] occur. The reflection and transmission for backward direction at two UPA points (1544.687nm and 1544.696nm) are both near 0 (see Fig. 2(a) and 2(d)). The absorptions at the two UPA points for backward direction are ~ 0.9 from the formula $A = 1 - |t|^2 - |r|^2$. And the corresponding quality factors of the UPAs are both ~ 309 by using the formula $f/\Delta f$ with f and Δf the resonant frequency and full width half maximum, respectively. When phase shift $\theta_1 = 1.03635\pi$, two UPAs (marked by two red arrows in Fig. 3(f)) for forward direction appear at 1554.9nm and 1555.1nm, respectively, with the absorptions of both ~ 0.9 and quality factors of ~ 311.

Figure 4 shows the real (a,c) and imaginary (b,d) parts of the eigenvalues $s_\pm$ as function of wavelength with different phase shift θ_1 and decay rate Γ. In Figs. 4(a) and 4(b), when $\Gamma = 0.2\eta$ ($\Gamma = 0.3\eta$) and phase shift $\theta_1 = 0.92824\pi$ ($\theta_1 = 0.8945\pi$), two real parts coalesce at one point while two imaginary parts cross at wavelength 1539.5nm (1534.4nm), which corresponds to the

Optics EXPRESS

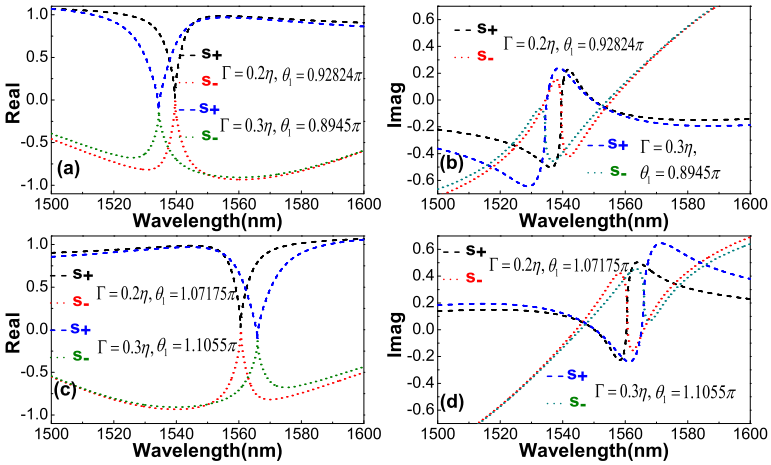

Fig. 4. Real (a,c) and imaginary (b,d) parts of the eigenvalues $s_{\pm}$ as the function of wavelength with different phase shift θ_1 and decay rate Γ.

same complex eigenvalues $s_+ = s_-$. That is, EPs occur at wavelength 1539.5nm and 1534.4nm when $\Gamma = 0.2\eta$ and $\Gamma = 0.3\eta$ for phase shift $\theta_1 = 0.92824\pi$ and 0.8945π, respectively. Also, from Figs. 4(c) and 4(d), two real parts coalesce at one point and two imaginary parts cross at wavelength 1560.5nm (1565.8nm) when $\Gamma = 0.2\eta$ ($\Gamma = 0.3\eta$) for phase shift $\theta_1 = 1.07175\pi$ ($\theta_1 = 1.1055\pi$), which corresponds to the same complex eigenvalues $s_+ = s_-$. That is, EPs appear. Compared Fig. 3 with Fig. 4, EPs take place blue-shift and red-shift with increasing the decay rate Γ when $\theta_1 < \pi$(see Fig.3(a) and 4(a)) and $\theta_1 > \pi$(see Fig.3(e) and 4(c)).

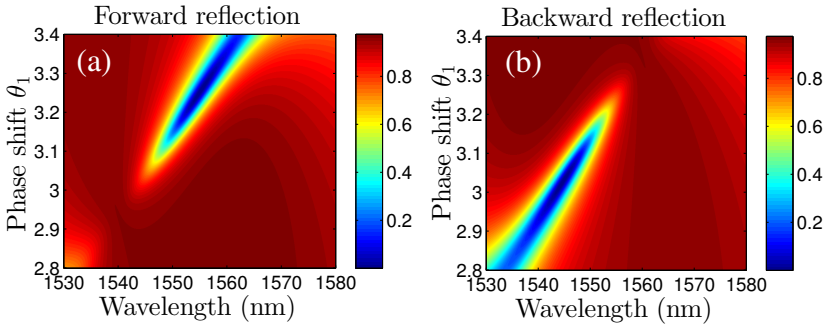

Fig. 5. Dependence of reflection on phase shift θ_1 and wavelength for forward (a) and backward (b) directions.

Figure 5 exhibits the influences of wavelength and phase shift θ_1 on reflections for forward and backward directions. From Figs. 5(a) and 5(b), unidirectional low reflection appears in the wavelength ranges of 1553nm~1561nm and 1540nm~1548nm, respectively, corresponding to phase shift ranges of $1.02\pi \sim 1.07\pi$ and $0.94\pi \sim 0.99\pi$ for forward and backward directions. In other words, the low reflection region (blue region) for forward direction (Fig. 5(a)) corresponds to high reflection region (red region) for backward direction (Fig. 5(b)), and vice versa. Therefore, the unidirectional low reflection can be achieved in the wide phase shift range and wavelength range.

Optics EXPRESS

4. Dual-band unidirectional reflectionlessness

Then we discuss the case of three unidentical QDs coupled to a plasmonic waveguide. By solving the eigenvalue equation $H|E_k\rangle = E_k|E_k\rangle$, we can get the transmission and reflection coefficients for forward and backward directions, as

$$t = \left[e^{2i\theta_1}(\Gamma - 2i\Delta_1)(\Gamma - 2i\Delta_2)(\Gamma - 2i\Delta_3)\right]/X, \tag{7}$$

$$\begin{aligned} r_f = \Big\{&64(-1 + e^{2i\theta_1})(e^{2i\theta_1} - e^{2i\theta_2})\eta^3 + 32e^{2i\theta_1}\eta^2\big[(-1 + e^{2i\theta_2})\Gamma + i\big(\Delta_2 - e^{2i\theta_2}(\Delta_1 + \Delta_2) \\ &+e^{2i\theta_1}(\Delta_1 - \Delta_3) + \Delta_3\big)\big] - 4\eta e^{2i\theta_1}\big[(1 + e^{2i\theta_1} + e^{2i\theta_2})\Gamma^2 - 4(e^{2i\theta_2}\Delta_1\Delta_2 + e^{2i\theta_1}\Delta_1\Delta_3 + \Delta_2\Delta_3) \\ &-2i\Gamma\big(\Delta_2 + e^{2i\theta_2}(\Delta_1 + \Delta_2) + \Delta_3 + e^{2i\theta_1}(\Delta_1 + \Delta_3)\big)\big]\Big\}/X, \end{aligned} \tag{8}$$

$$\begin{aligned} r_b = \Big\{&64(-1 + e^{2i\theta_1})(e^{2i\theta_1} - e^{2i\theta_2})\eta^3 + 32e^{2i\theta_1}\eta^2\big[(-1 + e^{2i\theta_2})\Gamma - i\big((-1 + e^{2i\theta_1})\Delta_1 \\ &+(-1 + e^{2i\theta_2})\Delta_2 + (-e^{2i\theta_1} + e^{2i\theta_2})\Delta_3\big)\big] - 4\eta e^{2i\theta_1}\big[(1 + e^{2i\theta_1} + e^{2i\theta_2})\Gamma^2 - 2i\Gamma(\Delta_1 + e^{2i\theta_1}\Delta_1 \\ &+\Delta_2 + e^{2i\theta_2}\Delta_2 + e^{2i\theta_1}\Delta_3 + e^{2i\theta_2}\Delta_3) - 4\big(e^{2i\theta_2}\Delta_2\Delta_3 + \Delta_1(\Delta_2 + e^{2i\theta_1}\Delta_3)\big)\big]\Big\}/X, \end{aligned} \tag{9}$$

where

$$\begin{aligned} X = &-64(-1 + e^{2i\theta_1})(e^{2i\theta_1} - e^{2i\theta_2})\eta^3 - 16\eta^2\Big\{e^{2i\theta_2}(\Gamma - 2i\Delta_1) + e^{2i(\theta_1+\theta_2)}(\Gamma - 2i\Delta_2) \\ &+ e^{4i\theta_1}(\Gamma - 2i\Delta_3) + e^{2i\theta_1}\big[-3\Gamma + 2i(\Delta_1 + \Delta_2 + \Delta_3)\big]\Big\} + 4\eta e^{2i\theta_1}\Big\{3\Gamma^2 - 4i\Gamma(\Delta_1 + \Delta_2 \\ &+ \Delta_3) - 4\big(\Delta_2\Delta_3 + \Delta_1\Delta_2 + \Delta_1\Delta_3\big)\Big\} + e^{2i\theta_1}(\Gamma - 2i\Delta_1)(\Gamma - 2i\Delta_2)(\Gamma - 2i\Delta_3), \end{aligned} \tag{10}$$

with θ_1 and θ_2 as the phase shifts between QD_1, QD_2 and QD_1, QD_3, respectively. Δ_3 is the detuning between QD_3 and incident surface plasmon.

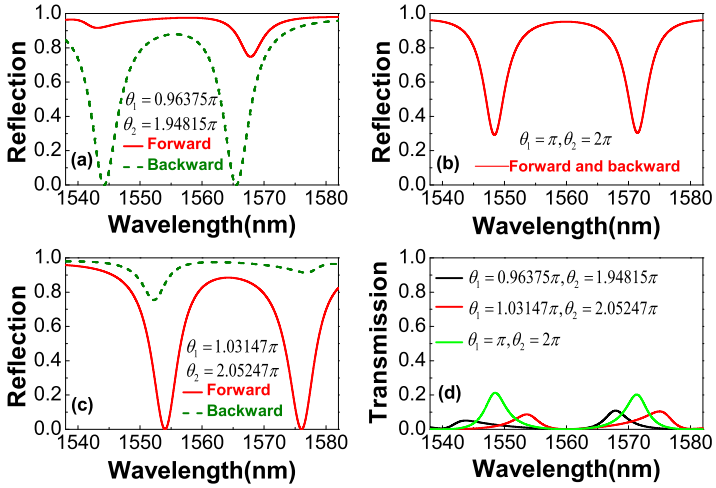

Fig. 6. Reflection spectra for forward and backward directions with different phase shifts $\theta_1 = 0.96375\pi, \theta_2 = 1.94815\pi$ (a), $\theta_1 = \pi, \theta_2 = 2\pi$ (b), and $\theta_1 = 1.03147\pi, \theta_2 = 2.05247\pi$ (c). (d) Transmission spectra with phase shifts $\theta_1 = 0.96375\pi, \theta_2 = 1.94815\pi$, $\theta_1 = \pi, \theta_2 = 2\pi$, and $\theta_1 = 1.03147\pi, \theta_2 = 2.05247\pi$, respectively. Here $\Gamma = 0.1\eta$, $\eta = 1.8 \times 10^{13}$rad/s.

Figure 6 shows reflection and transmission spectra versus wavelength for forward and backward directions with different phase shifts θ_1 and θ_2 by using Eqs. (7)-(10). From Fig. 6(a), when

Optics EXPRESS

phase shifts $\theta_1 = 0.96375\pi$ and $\theta_2 = 1.94815\pi$, reflections for forward (backward) direction are $\sim 0.9(\sim 0)$ and $\sim 0.88(\sim 0)$ at wavelength 1544.2nm and 1565.5nm, respectively. For phase shifts $\theta_1 = 1.03147\pi$ and $\theta_2 = 2.05247\pi$, reflections for forward (backward) direction are ~ 0 (~ 0.86) and ~ 0 (~ 0.91) at wavelength 1554nm and 1576nm, respectively, as shown in Fig. 6(c). Therefore, dual-band unidirectional reflectionless phenomenon at EPs appears by appropriate choosing phase shifts θ_1 and θ_2. From Fig. 6(b), reflections for forward and backward reflections are the same when phase shifts $\theta_1 = \pi$, $\theta_2 = 2\pi$. Fig. 6(d) shows the transmission spectra with different phase shifts θ_1 and θ_2, respectively. We notice that the transmissions for forward and backward directions are identical, and low transmissions appear at 1544.2nm (1554nm) and 1565.5nm (1576nm) when $\theta_1 = 0.96375\pi$ (1.03147π) and $\theta_2 = 1.94815\pi$ (2.05247π).

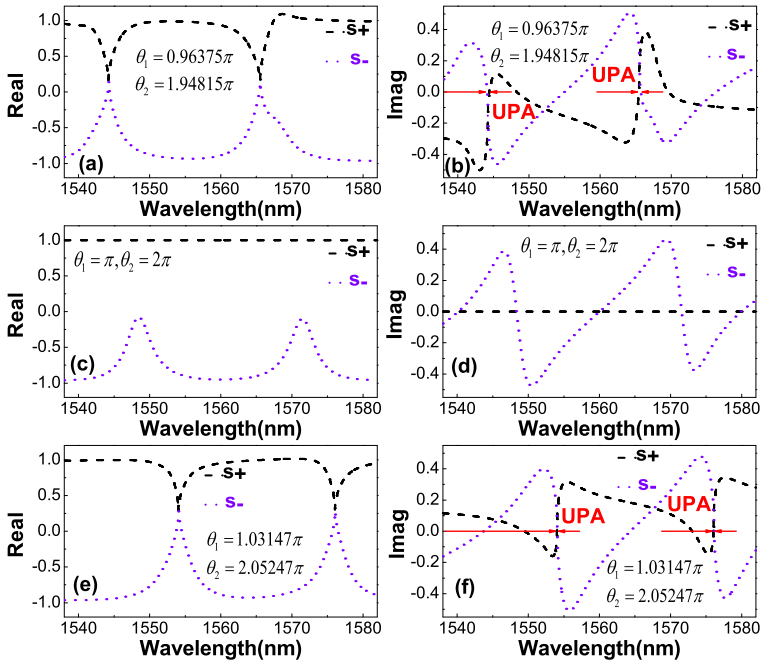

Fig. 7. The real (a,c,e) and imaginary (b,d,f) parts of the eigenvalues $s_\pm$ as the function of wavelength for different phase shifts $\theta_1 = 0.96375\pi$, $\theta_2 = 1.94815\pi$ (a,b), $\theta_1 = \pi$, $\theta_2 = 2\pi$ (c,d), and $\theta_1 = 1.03147\pi$, $\theta_2 = 2.05247\pi$ (e,f).

Figure 7 shows the real and imaginary parts of the eigenvalues $s_\pm$ of scattering matrix S as the function of wavelength. In Figs. 7(a) (7(e)) and 7(b) (7(f)), two real parts coalesce at two points while two imaginary parts cross at 1544.2nm (1554nm) and 1565.5nm (1576nm) when phase shifts $\theta_1 = 0.96375\pi$ (1.03147π) and $\theta_2 = 1.94815\pi$ (2.05247π), which corresponds to the same complex eigenvalues $s_+ = s_-$. That is, two EPs appear. Therefore, dual-band unidirectional reflectionlessness in our non-Hermitian quantum system is obtained by appropriate choosing the phase shifts between QDs (shown in Fig.6). From Figs. 7(c) and 7(d) for $\theta_1 = \pi$, $\theta_2 = 2\pi$, two real parts of $s_\pm$ do not coalesce and two imaginary parts are zero at wavelengths 1540.03nm, 1548.34nm, 1559.94nm, 1571.55nm and 1579.86nm, respectively. Correspondingly, t is real and $r_f r_b$ is bigger than zero. In this case, the system is Hermitian. Except for these points, the system is non-Hermitian. Therefore, phase transition from Hermitian to non-Hermitian occurs at 1540.03nm, 1548.34nm, 1559.94nm, 1571.55nm and 1579.86nm when $\theta_1 = \pi$, $\theta_2 = 2\pi$.

From Fig. 7(b) for $\theta_1 = 0.96375\pi$ and $\theta_2 = 1.94815\pi$, both imaginary parts of the eigenvalues $s_\pm$ are equal to zero at four points 1544.1nm, 1544.4nm, 1565.4nm and 1565.6nm (marked by

Optics EXPRESS

four red arrows), closed to EPs (1544.2nm and 1565.5nm), where UPAs appear. In view of that the reflections and transmissions for backward direction at 1544.1nm, 1544.4nm, 1565.4nm and 1565.6nm are near zero (see Figs. 6(a) and 6(d)), the absorptances of the four UPA points are all ~ 0.95. And the corresponding quality factors are all ~ 310. In addition, according to Fig. 7(f) for $\theta_1 = 1.03147\pi$ and $\theta_2 = 2.05247\pi$, UPA phenomena occur at 1553.9nm, 1554.1nm, 1575.9nm and 1576.1nm (marked by four red arrows), closed to EPs (1554nm and 1576nm), respectively. The absorptances of the four UPA points are all ~ 0.91 with the quality factors of ~ 260.

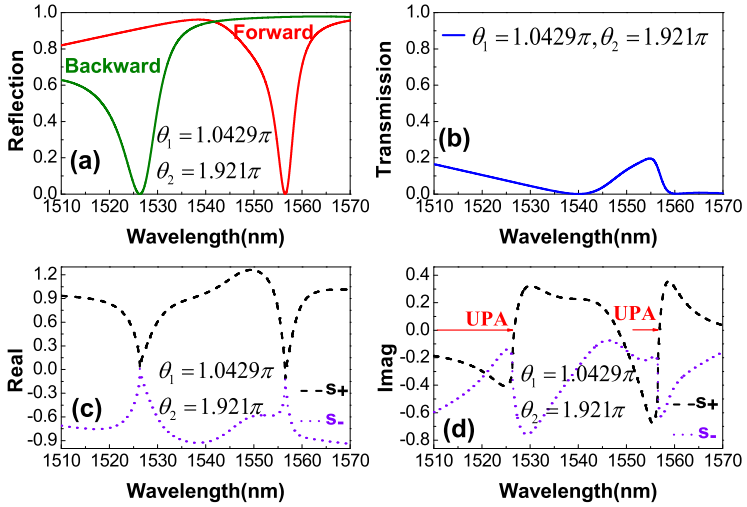

Fig. 8. When phase shifts $\theta_1 = 1.0429\pi, \theta_2 = 1.921\pi$, reflection spectra (a) and transmission spectra (b), as well as the real parts (c) and imaginary parts (d) of the eigenvalues $s_\pm$ as the functions of wavelength. Here $\Gamma = 0.0855\eta$, $\eta = 1.8 \times 10^{13}$ rad/s.

Figure 8(a) shows the reflection spectra for forward (red solid line) and backward (green solid line) directions when $\theta_1 = 1.0429\pi$ and $\theta_2 = 1.921\pi$. From Fig. 8(a), reflections for forward (backward) direction are ~ 0.91 (~ 0) and ~ 0 (~ 0.97) at 1526.3nm and 1556.5nm, respectively. Transmission spectrum (blue solid line) for $\theta_1 = 1.0429\pi$ and $\theta_2 = 1.921\pi$ is shown in Fig. 8(b), and low transmissivities occur at 1526.3nm and 1556.5nm. Figs. 8(c) and 8(d) exhibit the real and imaginary parts of the eigenvalues $s_\pm$ as the functions of wavelength when $\theta_1 = 1.0429\pi$ and $\theta_2 = 1.921\pi$, respectively. Apparently, two real parts coalesce at two points while two imaginary parts cross at 1526.3nm and 1556.5nm, respectively. In this case, the same complex eigenvalues $s_+ = s_-$ appear. It indicates that t is complex and $r_f r_b$ is zero. Therefore, dual-band unidirectional reflectionlessness at EPs is achieved when phase shifts $\theta_1 = 1.0429\pi$, and $\theta_2 = 1.921\pi$. From Fig. 8(d), the imaginary parts of the eigenvalues $s_\pm$ are equal to zero at two points 1526.7nm and 1556.9nm (marked by two red arrows), very closed to EPs (1526.3nm and 1556.5nm), which indicates the occurrence of UPAs. Together with the nearly-zero reflections for forward and backward directions (Fig.8(a)) and low transmissions (Fig.8(b)) at wavelength 1556.9nm and 1526.7nm, the corresponding absorptances of UPA peaks for forward and backward directions at 1556.9nm and 1526.7nm are of ~ 0.93 and ~ 0.87 with the quality factors of ~ 311 and ~ 153, respectively.

Recently, significant progresses for photon and surface plasmon coupling to QD in experiments have been achieved in photonic waveguide [38, 39] and silver nanowire waveguide [40], respectively, which increases the feasibility of our scheme with the current experiment technology.

Optics EXPRESS

5. Conclusion

We have demonstrated that single- and dual-band unidirectional reflectionless phenomena at EPs in non-Herimitian QDs-plamonic waveguide coupling system by appropriate adjusting the phase shifts between QDs. Moreover, unidirectional UPAs with the absorptances of ~ 0.95 and quality factors of ~ 310 are obtained near EPs. By generalizing the non-Hermitian system to n QDs-plasmonic waveguide coupling case, $(n-1)$-band unidirectional reflectionlessness can be obtained. We believe that our research results will have potential applications in the design of quantum devices such as diode-like, transistor, single plasmon switching, and so on.

Funding

National Natural Science Foundation of China (Grant No. 11364044); the Education Department of Jilin Province Science and Technology Research Projects (Grant No. JJKH20170455KJ)